The Astrophysical Journal, 671: L201–L204, 2007 December 20

THREE-DIMENSIONAL TOMOGRAPHIC ANALYSIS OF A HIGH-CADENCE LASCO-C2 POLARIZED BRIGHTNESS SEQUENCE

Richard A. Frazin
Department of Ocean, Atmospheric, and Space Science, University of Michigan, Ann Arbor, MI 48109; rfrazin@umich.edu
Alberto M. Vásquez
Instituto de Astronomía y Física del Espacio, CONICET–University of Buenos Aires, Argentina; albert@iafe.uba.ar
and
Farzad Kamalabadi and Hyesun Park
Department of Electrical and Computer Engineering, University of Illinois, Urbana, IL 61801; farzadk@uiuc.edu, hpark6@uiuc.edu
Received 2007 September 14; accepted 2007 October 31; published 2007 November 30

ABSTRACT

We present the first 3D tomographic reconstructions of the coronal electron density from an extended, high-cadence sequence of images of the corona's polarized brightness (pB). While the standard LASCO synoptic sequence is only 1 pB image per day, during the 14 day period covering 2006 June 9–22, the C2 coronagraph took about 6.5 pB images per day. We show that the high cadence dramatically improves the quality of the tomographic reconstructions when compared to a reconstruction that only uses one image per day. In particular, the reconstruction that uses only one image per day misses important features and has lower spatial resolution. We find that the spatial resolution of the tomographic inversion is ultimately limited by smearing due to coronal dynamics that take place during the 14 days required for data acquisition. We show that when only C2 images are available, about 4 pB images per day are enough for nearly optimal tomographic reconstruction, but more will be required when *STEREO* observations are included in the tomographic analysis.

Subject headings: Sun: corona — techniques: image processing

1. INTRODUCTION

Tomographic determination of the three-dimensional (3D) electron density (N_e) of the corona is of fundamental importance for a variety of scientific objectives ranging from accurate specification of the corona's background state for studies of shock acceleration of energetic particles to verification of solar wind models. The density structure of the corona strongly affects the propagation of CMEs (Riley et al. 2001; Odstrcil et al. 2002; Manchester et al. 2004). In particular, the density of the corona determines the amount of plasma swept up by the CME and its acceleration (Lugaz et al. 2005). The work of Odstrcil & Pizzo (1999) and Mancuso & Raymond (2004) has shown that CMEs have very significant interactions with streamer belt structures.

Solar rotational tomography (SRT) has emerged as a powerful technique for determining the 3D distribution of N_e from coronagraph images of the polarized brightness (pB). SRT was first performed by Altschuler & Perry (1972), and subsequent work has been reviewed in Frazin (2000) and Frazin & Janzen (2002; hereafter FJ02). SRT uses information provided by the range of view angles during 1/2 of a solar rotation to reconstruct N_e in the corona. Since 1/2 of a synodic rotation takes about 14 days, SRT is only capable of determining the slowly evolving background corona (which is dominated by large-scale structure). However, the launch of the *STEREO* mission (Howard et al. 2002) promises to decrease this time by as much as a factor of 3 (Frazin & Kamalabadi 2005a), allowing more accurate reconstructions.

During the 14 days spanning 2006 June 9–22, LASCO-C2 took between 6 and 7 pB sequences per day (roughly evenly spaced in time), resulting in 87 images that are useful as input for the tomographic analysis. This represents a cadence that is a factor of about 6.5 higher than the nominal cadence of 1 pB image per day. Our purpose is to take advantage of this data set in order to understand the relationship between coronagraph cadence and quality of the tomographic reconstructions.

While the 14 days (or less with *STEREO*) required for data collection is the method's most important limitation, one must also consider the rate at which pB images are taken within the time period. Ground-based coronagraphs, such as Mauna Loa Solar Observatory's Mk-IV coronagraph (Elmore et al. 2003), have short observing days (about 6 hr) and require good weather. Although Mk-IV may make as many as 120 pB images during the observing day, the fact that they are all confined to a short time period (instead of spread over 24 hr) limits their utility for SRT. In contrast, the COR1 and COR2 coronagraphs of the SECCHI package on the dual-spacecraft *STEREO* mission produce about 48 and 24 pB images per day, evenly distributed in time, respectively. The LASCO C2 and C3 coronagraphs (Brueckner et al. 1995) have a synoptic sequence that produces only 1 pB image per day, although the instruments are capable of producing pB sequences much more rapidly. The objective of this Letter is to argue that the objective of determining the 3D structure of the corona would be well served by increasing the LASCO synoptic pB rate, especially during the *STEREO* era.

A pB image is a combination of 3 images, each passing linearly polarized light at a different angle via polarizing optical elements (e.g., Billings 1966). Each set of 3 images is also known as a *pB sequence*. Note that a pB sequence can provide both the pB and total brightness (B) parts of the corona's emission (these, respectively, are the Q and I components of the Stokes vector in an appropriate coordinate system [Collett 1993; Frazin & Kamalabadi 2005b]). For the purposes of quantitative determination of N_e in the corona, pB images are preferred because the dust-scattered F-corona does not contribute significant uncertainty to the pB value at low heights. This is because F-corona emission at optical wavelengths is essentially unpolarized at low heights, while the electron-scattered K-co-

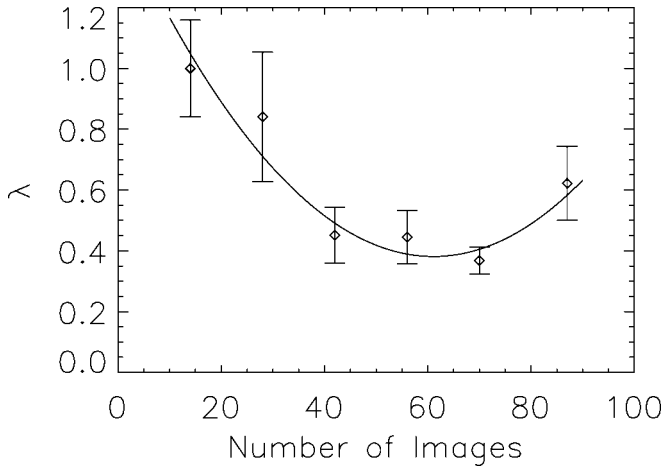

FIG. 1.—Regularization parameter as a function of the number of images used in the reconstruction in the 2 week observing period. Each point was determined via a cross-validation procedure similar to that described in FJ02. The value of each point is an average of the cross validation values for the individual images and the error bars are the square roots of the population variances. A parabolic fit to the regularization parameters is shown as a visual aide.

rona is known to be strongly polarized with the electric field vector oscillating in a plane parallel to the limb tangent (e.g., Billings 1966; Kimura & Mann 1998). Blackwell & Petford (1966a, 1966b; also see Mann 1992) used spectroscopic separation of the F and K components to show that the F corona is about 0.2% polarized at 10 $R_\odot$ and 0.5% polarized at 15 $R_\odot$. More recently, Moran has reconfirmed that the K-corona dominates the polarized intensity below 6 $R_\odot$ (Moran et al. 2006). Thus, tomographic reconstructions from pB images below about 6 $R_\odot$ are not significantly contaminated by the F-corona.

While the *STEREO* coronagraphs continuously run pB sequences in their standard observing mode, the vast majority of the images produced by LASCO coronagraphs are taken without polarizing elements in the optical path (the slight circular polarization imposed by the C2 optics not withstanding; see the calibration paper by Moran et al. 2006). Independently of how the coronagraph data are used, whether it is for SRT or other analysis, it seems obvious that in order to take full advantage of the unique opportunity provided by concurrent operations of the *SOHO* and *STEREO* missions, a LASCO observing mode that more closely matches that of COR1 and COR2 would be desirable. We show that the 3D N_e reconstructions produced by SRT would benefit greatly from an increased synoptic rate.

The N_e value is related to the pB seen in the jth coronagraph image pixel by a line-of-sight (LOS) integral (van de Hulst 1950):

$$y_j = \int_{-\infty}^{\infty} w[\boldsymbol{r}_j(l)] N_e[\boldsymbol{r}_j(l)] dl, \qquad (1)$$

where y_j is the pB value of the pixel in question, $\boldsymbol{r}_j(l)$ is a vector that traces the LOS as a function of distance l, and $w(\boldsymbol{r})$ is a weighting function given by the physics of the Thomson scattering process. Equation (1) comes from the radiative transfer equation in the optically thin limit. A system of equations, each equation of the form of equation (1), can be inverted to determine $N_e(\boldsymbol{r})$ after the Sun has rotated through about 180° for a single observer. This can be decreased to as little as 60° of solar rotation when the *SOHO* + *STEREO* geometry is optimal.

Let the vector $\boldsymbol{x}$ be a discrete representation of N_e (e.g., each element of $\boldsymbol{x}$ can represent the value of N_e in a particular volume element of the computation grid). Note that since the $\boldsymbol{x}$ vector represents a 3D object, it will typically have hundreds of thousands or millions of components. Now consider the vector $\boldsymbol{y}$ which contains all of the pB values, i.e., if there are N pB images each with M pixels, the vector $\boldsymbol{y}$ will have NM elements. The vector $\boldsymbol{y}$ is related to $\boldsymbol{x}$ via $\boldsymbol{y} = \boldsymbol{A}\boldsymbol{x} + \boldsymbol{n}$, where the $\boldsymbol{A}$ matrix is calculated from equation (1) and $\boldsymbol{n}$ represents noise in the data. The vector of electron densities $\boldsymbol{x}$ exists in a coordinate system that rotates with the Sun and $\boldsymbol{A}$ must account for the transformations that relate the coronagraph images to the corotating coordinate system, taking the spacecraft orbital geometry and solar-pole tilt angle into account (FJ02). While FJ02 and Butala et al. (2005) calculated the first tomographic reconstructions from LASCO data on a cylindrical grid, the reconstructions shown here were calculated on a spherical grid with bins that are equally spaced in latitude, longitude, and radius.

It is solar rotation and multispacecraft view angles that provide enough information to make the matrix $\boldsymbol{A}$ nearly invertible. This a nontrivial problem due to the large size of the matrix $\boldsymbol{A}$ and its ill-conditioned (and/or underdetermined) nature. As described in Frazin (2000) and FJ02, a procedure called *regularization*[1] (e.g., Tikhonov 1977) gives a unique solution that is stable to measurement noise.

We note that not only do the reconstructions on the spherical grid look superior to those on the cylindrical grid; there is large computational savings because the spherical grid requires us to determine only one regularization parameter instead of three. Thus, the regularized tomographic solution is given by (FJ02) $\boldsymbol{x}(\lambda) = \mathrm{argmin}_x(\|\boldsymbol{y} - \boldsymbol{A}\boldsymbol{x}\|^2 + \lambda^2\|\boldsymbol{R}\boldsymbol{x}\|^2)$, where λ is the regularization parameter and the $\boldsymbol{R}$ matrix is a finite difference approximation to the operator $(\partial^2/\partial\theta^2, \partial^2/\partial\phi^2)^T$ (where the superscript T denotes transpose). No smoothness constraint is needed for the radial direction because the regularization scheme we use is sufficient to stabilize the system of equations.

2. RESULTS AND DISCUSSION

As the goal of any regularization procedure is to provide physically plausible solutions that are consistent with the data, one might expect the value of the regularization parameter λ to be function of the number of images, allowing increased complexity in the solution as the number of images increases (up to a saturation point; see below). In order to examine this trend, we created a series of reconstructions with 14, 28, 42, 56, 70, and 87 images, each with approximately evenly spaced observations throughout the 14 days spanning 2006 June 9–22. For each of these reconstructions a value of λ was determined using a (one-dimensional) cross validation procedure similar to that described in FJ02. The (normalized) regularization parameters for each of these are shown in Figure 1.

In "standard" tomographic reconstruction problems (e.g.,

[1] Regularization is a method for stabilizing the large system of linear equations encountered in the tomographic inversion. It requires the solutions to be spatially smooth. The regularization parameter controls the strength of the regularization. If the parameter is too large, the reconstruction will be too smooth and not agree with the coronagraph data to within acceptable limits. However, if it is too small, the reconstruction will agree with the coronagraph data quite well but not be physically reasonable and will exhibit unrealistic oscillations.

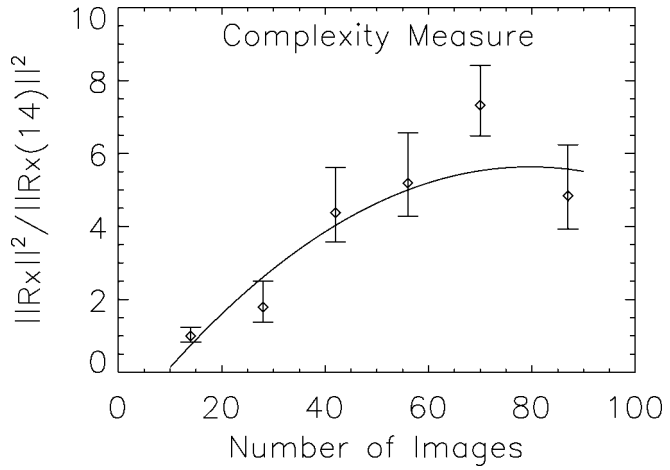

FIG. 2.—Complexity in the solution as a function of the number of images, using regularization parameters from Fig. 1. Note that according to the fitted parabolic curve, the complexity does not increase much beyond 56 images (corresponding to 3 images per day). The error bars are propagated from Fig. 1.

many medical imaging problems) in which the unknown object is unchanging with time, the information available is proportional to the number of view angles.[2] Hence, the spatial resolution of the reconstruction is proportional to the number of view angles for static objects (Kak & Slaney 1987). However, one of the effects of coronal dynamics in the 14 day time period is smearing of features (Frazin 2000; Frazin & Kamalabadi 2005a). It is this smearing caused by dynamics that imposes a fundamental limit on the spatial resolution that can be achieved by tomographic reconstructions of the solar corona.

In order to evaluate the effect of the number of images on the spatial resolution, we define a complexity measure $\mathcal{C}(\boldsymbol{x}) \equiv \|\boldsymbol{R}\boldsymbol{x}(\lambda)\|^2$. Note that the matrix $\boldsymbol{R}$ is the regularization matrix used in the reconstructions and $\mathcal{C}(\boldsymbol{x})$ increases as the solution has more gradients (thus, more features and higher spatial resolution). Figure 2 shows the complexity measure as a function of the number of images, using the regularization parameters from Figure 1. The parabolic fit to the complexity measure matches the data points to within the uncertainties and shows the saturation effect described above. Note that the fitted curve increases very little above 56 images, indicating that at least for this particular case, having more than about 4 pB images per day would not improve the solution very much. This result should be compared to repeated studies to verify the conclusions. The number of pB images required to adequately support the *STEREO* mission is likely to be higher for reasons discussed below.

It is instructive to compare a reconstruction made with the standard synoptic rate of 1 image per day, henceforth called "R14," to the reconstruction made with all 87 images, "R87." R87 represents the results of a high-cadence data set, while R14 represents a reconstruction made with the usual synoptic data set. The R87 reconstruction shows more contrast and more features than the R14 reconstruction because the larger number of images decreases the reliance on regularization to provide a physically plausible solution.

Figures 3 and 4 show the value N_e as a function of latitude and longitude on spherical shells at 2.55 and 5.00 $R_\odot$. The top panel of each figure shows a slice of R87 while the bottom shows R14. The superiority of the quality of the R87 reconstruction relative to that of R14 is evident in two major aspects:

[2] This can be verified by creating a fine grid in the object space and comparing the spectrum of singular values for discrete representations of the Radon operator for varying numbers of view angles.

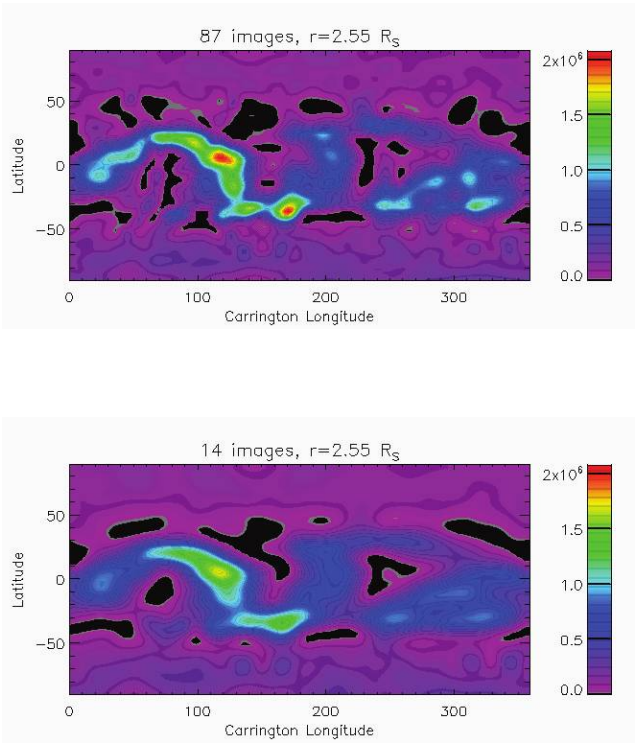

FIG. 3.—Comparison of the high-cadence reconstruction "R87" (*top*), made with 87 pB images, with a reconstruction made with only 14 pB images "R14" (*bottom*), which is the standard synoptic rate for LASCO. Each panel represents the electron density, in units of cm^{-3}, on a spherical shell with radius $r = 2.55\ R_\odot$. In each panel the *x*-axis is the Carrington longitude and the *y*-axis is the latitude. As discussed in the text, R87 exhibits a considerably higher spatial resolution than R14 and therefore shows more features. The differences at larger heights are more obvious, as can be seen in Fig. 4. The black regions are artifacts in which the reconstruction gives a density of 0, and probably are caused by coronal dynamics (see text).

1. R14 has a significantly lower spatial resolution, missing many structures that appear in R87. This poorer resolution increases with height. For example, in Figure 3 one may compare R87 and R14 around the following points [(latitude, longitude)]: (10, 40), (10, 100), (−30, 150), and (−30, 270). In each case R87 exhibits several high-density "islands" that are smeared together into a singly-peaked structure with less contrast in R14. As can be seen in Figure 4, the lack of spatial resolution in R14 becomes even more drastic at larger heights, where structures that are spatially much more separated are unresolved by R14. For example, in Figure 4 the two high-density well-separated "islands" at points (−20, 270) and (0, 310) seen in R87 are merged into a single-peak structure around point (−10, 295) in R14. As another example, also in Figure 4, multiple density islands that appear in R87 between Carrington longitudes 40 and 100, and latitudes −30 and 20, are missed by R14 and merged into much simpler structures in R14.

2. R14 underestimates the density contrast between the streamers and the background and the maximum streamer densities, an effect that also increases with height. For example, in Figure 3 the streamer high-density peaks of R87 around the points (10, 118), (−33, 172), and (−30, 320) present values of 2.0×10^6, 2.1×10^6, and 1.2×10^6 cm^{-3}, respectively. In

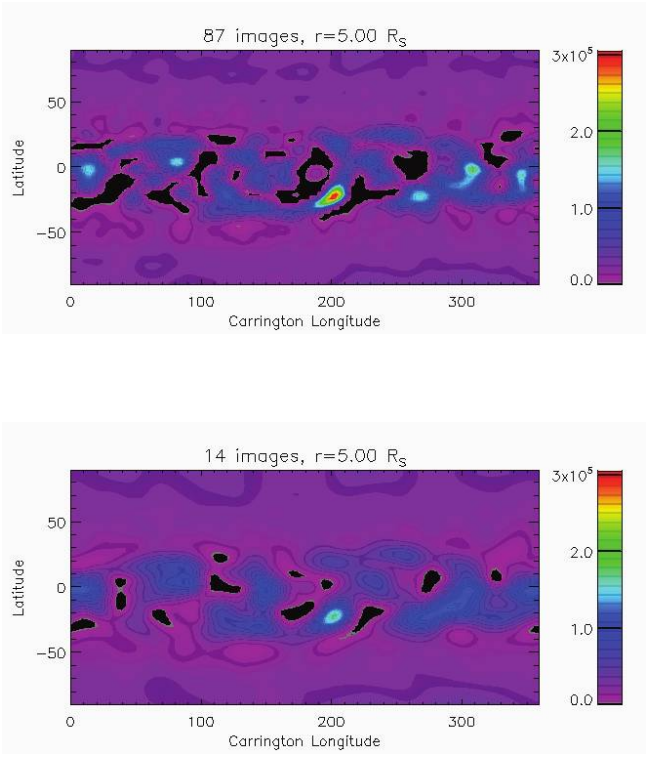

FIG. 4.—Similar to Fig. 3, except at $r = 5.53\ R_\odot$. At this height the differences between R87 and R14 are more pronounced than in Fig. 3. Differences between these two images are discussed in the text.

R14, these same regions exhibit peak values of 1.8×10^6 (or 10% lower), 1.4×10^6 (or 35% lower), and 9.0×10^5 cm^{-3} (or 33% lower), respectively. At larger heights the differences are even greater. In Figure 4, the streamer high-density peaks of R87 around the points (−20, 200), (0, 310), and (0, 345) present values of 3.0×10^5, 1.8×10^5, and 1.6×10^5 cm^{-3}, respectively. In R14, these same regions exhibit peak values of 1.7×10^5 (or 75% lower), 1.1×10^5 (or 65% lower), and 1.0×10^5 cm^{-3} (or 60% lower), respectively.

The black regions shown in Figures 3 and 4 represent regions of zero density in the reconstruction, so called "zero-density artifacts" (ZDAs). These are likely to be caused by coronal dynamics (FJ02; Frazin & Kamalabadi 2005a). This effect seems to be roughly equally important in R14 and R87. The shorter data acquisition times allowed by *SOHO* + *STEREO* observations should reduce their importance significantly.

This discussion naturally leads to the question: What should the synoptic pB rate of a space-based coronagraph near the Earth be? The results of this study indicate that when the Sun is observed by only by the C2 coronagraph, it is likely that more than about 4 pB images per day are not necessary for tomography. However, when *STEREO* + *SOHO* observations are available, a full set of data will be acquired in a little as 4.5 days, allowing much less time for the Sun to change than during 14 days, and therefore producing much less smearing in the reconstructions. Thus, one would expect the spatial resolution limit set by coronal dynamics to be less severe and more than 4 images per day should be acquired. We restate the argument that while the *STEREO* mission is in operation, it would be ideal for such an instrument to produce pB images at a rate comparable to the COR1 and COR2 coronagraphs in order to have compatible data sets from all 3 points of view. Such a data set would be useful for a great variety of studies, such as the 3D CME reconstructions via the method of Moran & Davila (2004), and it would certainly be beneficial for the type of tomographic analysis presented here. We note that methods for time-dependent tomography also will help to mitigate the effects of coronal dynamics on tomographic reconstruction (Frazin et al. 2005).

Perhaps the best way to determine the best C2 cadence for the *STEREO* era would be an approach similar to the one presented in this Letter. One could design a LASCO campaign with a 1 hr pB rate and perform *SOHO* + *STEREO* reconstructions using all, one-half, one-fourth, etc., of the data, compute complexity measures, and compare the results. It is possible that more active periods in the solar cycle would require more data. It may be that such a large pB rate would require too much telemetry, in which case lower resolution options (binning the detector pixels) should be explored.

This research was supported by the NSF SHINE and CMG programs, awards 0555561 and 0620550, respectively, to the University of Illinois. A. M. V. acknowledges CONICET grant PIP 6220 to IAFE for partial support. We would like to thank Philip Judge for insightful questions that helped us improve the manuscript.

REFERENCES

Altschuler, M. D., & Perry, R. M. 1972, Sol. Phys., 23, 410
Billings, D. E. 1966, A Guide to the Solar Corona (New York: Academic)
Blackwell, D. E., & Petford, A. D. 1966a, MNRAS, 131, 383
———. 1966b, MNRAS, 131, 399
Brueckner, G. E., et al. 1995, Sol. Phys., 162, 357
Butala, M. D., Frazin, R. A., & Kamalabadi, F. 2005, J. Geophys. Res., 110, A09S09
Collett, E. 1993, Polarized Light: Fundamentals and Applications (New York: Marcel Drekker, Inc.)
Elmore, D. F., Burkepile, J. T., Darnell, J. A., Lecsinki, A. R., & Stanger, A. L. 2003, Proc. SPIE, 4843, 66
Frazin, R. A. 2000, ApJ, 530, 1026
Frazin, R. A., Butala, M. D., Kemball, A., & Kamalabadi, F. 2005, ApJ, 635, L197
Frazin, R. A., & Janzen, P. 2002, ApJ, 570, 408
Frazin, R. A., & Kamalabadi, F. 2005a, Sol. Phys., 228, 219
———. 2005b, ApJ, 628, 1061
Howard, R. A., Moses, J. D., Socker, D. G., Dere, K. P., & Cook, J. W. 2002, Adv. Space Res., 29, 2017
Kak, A. C., & Slaney, M. 1987, Principles of Computerized Tomographic Imaging (New York: IEEE)
Kimura, H., & Mann, I. 1998, Earth Planets Space, 50, 493
Lugaz, N., Manchester, W. B., IV, & Gombosi, T. I. 2005, ApJ, 627, 1019
Manchester, W., IV, Gombosi, T., Ridley, A., Roussev, I., DeZeeuw, D. L., Sokolov, I., Powell, K., & Tóth, G. 2004, J. Geophys. Res., 109, A02107
Mancuso, S., & Raymond, J. C. 2004, A&A, 413, 363
Mann, I. 1992, A&A, 261, 329
Moran, T. G., & Davila, J. M. 2004, Science, 305, 66
Moran, T. G., Davila, J. M., Morrill, J. S., Wang, D., & Howard, R. 2006, Sol. Phys., 237, 211
Odstrcil, D., Linker, J., Lionello, R., Mikić, Z., Riley, P., Pizzo, V., & Luhmann, J. 2002, J. Geophys. Res., 107, 1493
Odstrcil, D., & Pizzo, V. J. 1999, J. Geophys. Res., 104, 493
Riley, P., Linker, J. A., & Mikić, Z. 2001, J. Geophys. Res., 106, 15889
Tikhonov, A. N. 1977, Solutions of Ill-posed Problems (New York: Wiley)
van de Hulst, H. C. 1950, Bull. Astron. Inst. Netherlands, 11, 135